Eur. Phys. J. A **18**, 645–651 (2003)
DOI 10.1140/epja/i2003-10089-y

THE EUROPEAN PHYSICAL JOURNAL A

Data on light-fragment correlations in ^{40}Ar + ^{58}Ni at 77 MeV/nucleon

K. Mikhailov[1,a], A. Stavinskiy[1], J.C. Angelique[2], B. Benoit[3], E. de Goes Brennand[3], G. Bizard[2], J. Colin[2], G. Costa[4], P. Désesquelles[5], O. Dorvaux[4], D. Durand[2], B. Erazmus[6], Yu. Grishuk[1], F. Hanappe[3], A. Kieliszek[7], S. Kuleshov[1], C. Lebrun[6], R. Lednicky[8], G. Leksin[1], P. Leszczynski[7], M. Marques[2], Th. Materna[3], K. Miller[7], G. Papatheofanous[3], T. Pawlak[7], J. Pluta[7], M. Przewlocki[7], A. Staranowicz[7], L. Stuttge[4], B. Tamain[2], A. Vlasov[1], L. Vorobyev[1], and K. Wosinska[7]

[1] Institute of Theoretical and Experimental Physics, B. Cheremushkinskaya 25, 117259, Moscow, Russia
[2] Laboratoire de Physique Corpusculaire, IN2P3, CNRS/ISMRA, F-14050 Caen Cedex, France
[3] Université Libre de Bruxelles, CP 229, Av. F.D. Roosevelt, 50, B-1050, Bruxelles, Belgium
[4] IRES, IN2P3-CNRS/Université Louis Pasteur, BP 28, F-67037 Strasbourg Cedex 2, France
[5] ISN, IN2P3/CNRS, et Université J. Fourier, 53 Av. des Martyrs, F-38026 Grenoble Cedex, France
[6] SUBATECH, UMR Université, EMN, IN2P3/CNRS, 4 rue A. Kastler, F-44307 Nantes, France
[7] Faculty of Physics, Warsaw University of Technology, Koszykowa 75, PL-00-662 Warsaw, Poland
[8] Institute of Physics ASCR, Na Slovance 2, CZ-18221 Prague 8, Czech Republic

Received: 26 May 2003 /
Published online: 2 December 2003 –
Communicated by V.V. Anisovich

Abstract. Results of the experimental study of p ^{4}He, d ^{3}He, dT, pT, p ^{3}He and, for the first time, nT, n ^{3}He, n ^{4}He correlations in the region of small relative momenta are presented. The data analysis provides an estimate of the effective source size or emission time.

PACS. 25.70.Pq Multifragment emission and correlations

1 Introduction

The study of the space-time characteristics of particle emission is important for understanding the reaction mechanism, particularly, the mechanism of heavy-ion collisions. The conventional method to determine the space-time characteristics of the reaction is based on a study of particle correlations at small relative momenta [1–4]. The behaviour of the correlation function is basically determined by the effects of the quantum-statistical interference and the strong and Coulomb interaction in the final state. Since these effects depend on the space-time separation of the emission points, the shape of the correlation function reflects the space-time size of the particle source.

The study of the correlation functions of pions, kaons and protons proved to be very useful for understanding the underlying production mechanism. The extension of the method to the correlations of neutrons and light nuclear fragments can provide a new valuable information on the space-time characteristics of the reactions. The application of this technique is however connected with some difficulties related mainly with the uncertainties in the description of the strong final-state interaction between light nuclear fragments. We hope that the comparison of the correlation functions for isosymmetrical systems will help to clarify the role of the quantum statistics and the Coulomb and strong final-state interaction contributions for these systems. This work is devoted to study the correlations in p ^{4}He and n ^{4}He, d ^{3}He and dT, p ^{3}He and nT, n ^{3}He and pT systems in the reaction ^{40}Ar + ^{58}Ni at 77 MeV/nucleon.

2 Experimental setup and data sample

The experiment (E286) was performed at GANIL (France) using the experimental setup DEMON (Detectour Modulaire de Neutron) [5]. The module of the detector was a combination of the main and additional scintillation counters. The main counter was an aluminum cylinder of 16 cm in diameter and 20 cm in length filled with the liquid scintillator NE213. This counter registered and identified both neutrons and charged particles. The technique of the neutron registration in coincidence was described in [6]. The additional counter —the thin (3 mm) plastic scintillator

[a] e-mail: kmikhail@itep.ru

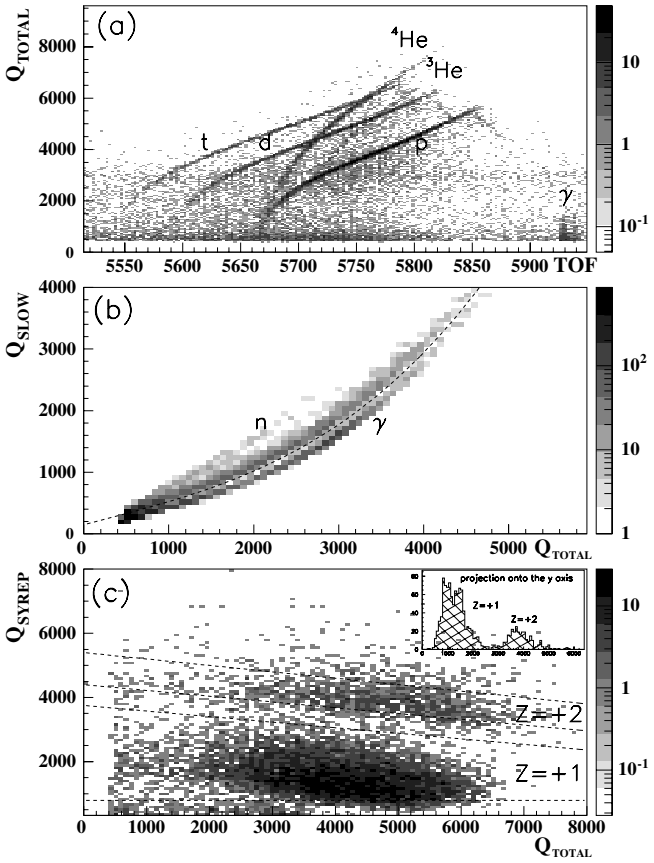

Fig. 1. Particle identification.

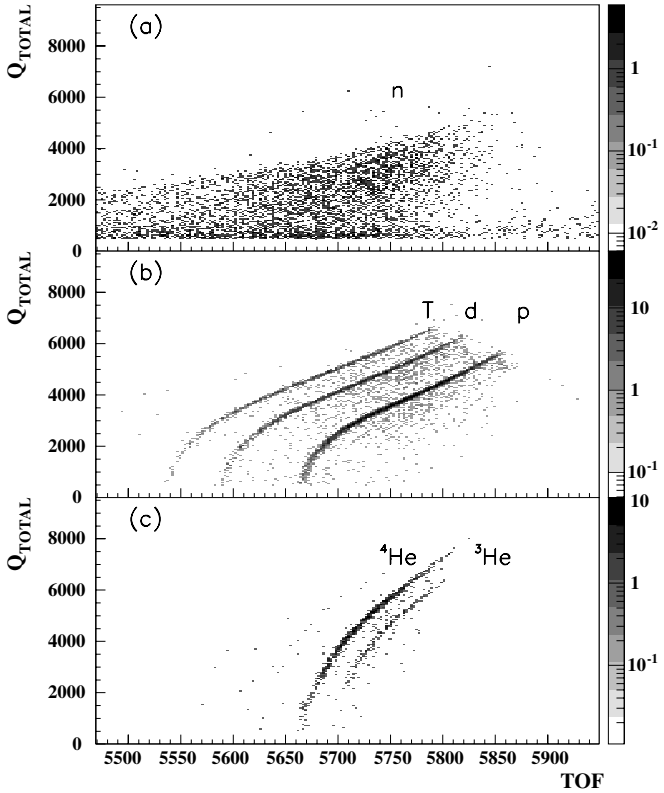

Fig. 2. Results of particle identification.

(SYREP —System de Rejection de Proton)— was located in front of the face of the main counter. There were two purposes for the SYREP operation. First, it provided the veto signal for neutral particles. Second, it allowed for the separation of charged particles with charge +1 and +2. The amplitude and time-of-flight signals from both parts of the module give us the possibility of particle identification and energy measurement. The difference between the shape of the signals for a neutron and for a photon was used to select neutrons.

A compact block of the modules was placed at the polar angle $\Theta = 4°$–$22°$. It allowed us to enrich the number of pairs with small relative momenta. A detailed description of the experimantal setup can be found elsewhere [7]. The typical time-of-flight (TOF in arbitrary units) dependence of the total charge (Q_{TOTAL} in arbitrary units) in the main DEMON detector for all registered particles is shown in fig. 1a. One can see the strips corresponding to charged particles —protons, deuterons, tritons, ^{3}He and ^{4}He. Figure 1b illustrates the separation of neutrons and photons using the individual cut curve for every module.

The separation of the charged particles with $Z = 1$ and $Z = 2$ is shown in fig. 1c. The dependence of the total charge in SYREP (Q_{SYREP} in arbitrary units) *versus* Q_{TOTAL} shows two regions, corresponding to the particles with charge $Z = 1$ and $Z = 2$. Margin cuts for different charged particles were defined individually for every module of the DEMON detector.

The results of the separation of the particle species are presented in fig. 2a, b, c for the same module of DEMON detector as in the previous figure. Figure 2a demonstrates a clean neutron selection. Figure 2b shows the selection of the particles with charge $Z = 1$. Three different strips correspond to proton, deuteron and triton.

The selection of the particles with charge $Z = 2$ is shown in fig. 2c.

The resolution expressed in the relative momentum k^* in the pair CMS is about 6 MeV/c. The contamination of particles with $Z = 1$ in particles with $Z = 2$ is less than 5%.

The start signal for data acquisition system was taken from the coincidence of any two incoming signals from main counters.

The possibility of a simultaneous registration of $Z = 1$, $Z = 2$ particles and neutrons is unique for such type of experiment.

To get approximately the same kinematical region for different particle species we apply the cut $\Theta < 110°$ in the projectile system. The mean kinetic energy and angle of the particle pairs at $k^* < 0.1$ GeV/c (the region of the correlation effect) in LAB and ANTILAB systems are shown in table 1.

Figure 3 illustrates an example of the neutron spectrum $\left(\frac{1}{p}\frac{\mathrm{d}N}{\mathrm{d}E_{\mathrm{KIN}}}\right)$ for typical detector module ($\Theta = 5°$ in LAB system) as a function of E_{KIN} multiplied by the sign of the Z-component of the particle momentum (all variables are in the projectile system). Peaks in the regions

Table 1. The mean kinetic energy and angle of the particle pairs at $k^* < 0.1$ GeV/c in the LAB (ANTILAB) system.

Pairs	E_1 (MeV)	E_2 (MeV)	Θ_1	Θ_2
p ^{4}He	98(5.6)	377(15.6)	10.9°(67°)	9.2°(66°)
n ^{4}He	90(4.8)	364(14.4)	11.2°(77°)	9.2°(70°)
nT	91(4.8)	267(11.2)	10.9°(75°)	9.9°(75°)
p ^{3}He	101(6.2)	298(15.8)	10.9°(65°)	10.0°(64°)
pT	97(5.7)	270(12.3)	11.1°(69°)	10.2°(74°)
n ^{3}He	93(5.1)	293(14.7)	10.8°(73°)	9.9°(65°)
dT	181(8.5)	264(11.4)	10.5°(74°)	10.2°(76°)
d ^{3}He	190(10.0)	288(14.2)	10.6°(70°)	10.0°(67°)

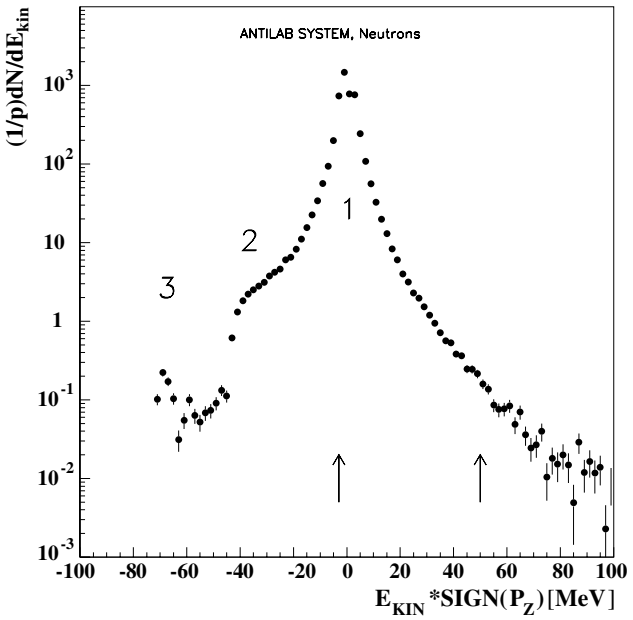

Fig. 3. Neutron spectrum in the projectile system for typical detector module ($\Theta = 5°$).

1 and 3 correspond to the fragmentation of nuclei ^{40}Ar and ^{58}Ni, respectively. Their relative amplitude is determined not only by physical reasons but also by the acceptance of the detector module. The bump in region 2 can be linked to a compound-nucleus production. Two arrows show the energy range (about 60–250 MeV in the LAB system) chosen for the analysis. One can see that this energy range corresponds to the ^{40}Ar fragmentation region. Both the mean value of the particle kinetic energy ($\sim$ 5 MeV/nucleon) and the mean value of the slope parameter for energy spectra ($\sim$ 10 MeV) indicate the importance of the evaporation mechanism in the chosen energy range.

3 Results

The correlation function R is the ratio of the semi-inclusive two-particle production cross-section to the product of the single-particle production cross-sections. We study R as a function of the effective mass M_{12} or the particle momentum in the pair rest frame $\boldsymbol{k}^* = \boldsymbol{p}_1^* = -\boldsymbol{p}_2^*$.

Our main interest is the correlation function shape at small k^* —less than 0.1 GeV (or M_{12} near threshold). At larger k^* ($k^* > 0.15$ GeV/c) the correlation function is close to a constant, and we will not pay attention to its absolute value.

Following the well-known procedure (see, for example, [8]), the correlation function can be calculated as a ratio of the measured distribution (on k^* or M_{12}) to the artificial (mixed) one constructed by the so-called mixing procedure [9].

To explain this procedure, let us consider the calculation of the neutron-alpha correlation function:

a) The events with neutron + α-particles were selected using some physical and methodical criteria.

b) Information about both particle characteristics was stored in a buffer. The size of the buffer was selected to be large enough in order to have statistical errors of the mixed distributions much smaller than those of the real ones.

c) Arbitrary neutrons and alphas, detected by different DEMON modules were selected from the buffer.

If these particles were from the same event, the information was used to fill the real distributions, otherwise, the mixed ones.

d) The real to mixed distribution ratio was normalized so that the mean value of this ratio at $0.15 < k^* < 0.30$ GeV/c was equal to 1.

The effective-mass dependences of the experimental correlation functions for p ^{4}He and n ^{4}He, for nT and p ^{3}He, for pT and n ^{3}He, for dT and d ^{3}He are plotted in fig. 4, and figs. 6, 8, 10 below. The reason for plotting those pairs in the same figure is that the sums of the fragments represent the isotope-symmetric nuclei with four or five nucleons. The justification for such a kind of analysis is the similarity of the excitation spectra of isotope-symmetric nuclei. The chosen pairs show similar behaviour. Below we shall discuss every pair in more detail. For (d ^{3}He, pα, pT and dT) pairs, similar results can also be found in [10,11]. The data for the same pairs and also for the pair p ^{3}He were studied in [12] at energy 400 MeV/nucleon.

The effective-mass dependence of the p ^{4}He and n ^{4}He correlation functions is shown in fig. 4. Here and below the full symbols and solid lines correspond to the pair with higher summary charge. For example, in fig. 4 the full circles show the experimental p ^{4}He correlation function, the solid arrow shows the threshold of the p ^{4}He pair production, vertical solid arrows with horizontal solid double arrows represent the energy levels and the widths of the ^{5}Li nucleus, respectively. The positions of the maxima of the p ^{4}He and n ^{4}He correlation functions correspond to the ground states of ^{5}Li and ^{5}He nuclei [13]. The energy levels of these nuclei are approximately the same. Higher-energy levels do not show up in the correlation functions. To the right of the peaks both correlation functions are reduced to constants. The value of the peak of the n ^{4}He correlation function is higher than p ^{4}He due to the absence of the Coulomb repulsion [3].

The ratio of the p ^{4}He and n ^{4}He correlation functions is shown in fig. 5. This ratio is compared with the

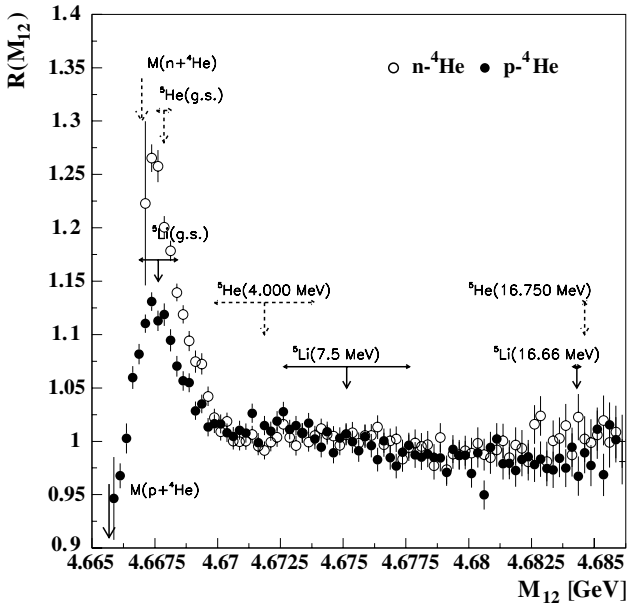

Fig. 4. The effective-mass dependence of the p ^{4}He and n ^{4}He correlation functions.

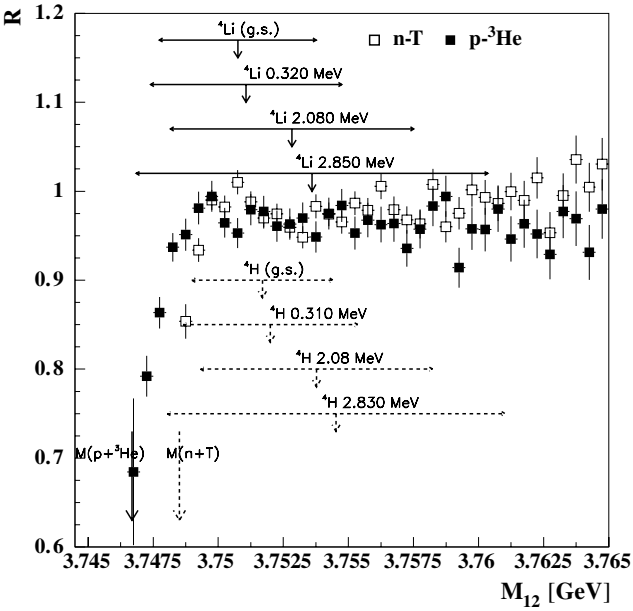

Fig. 6. The effective-mass dependence of the nT and p ^{3}He correlation functions.

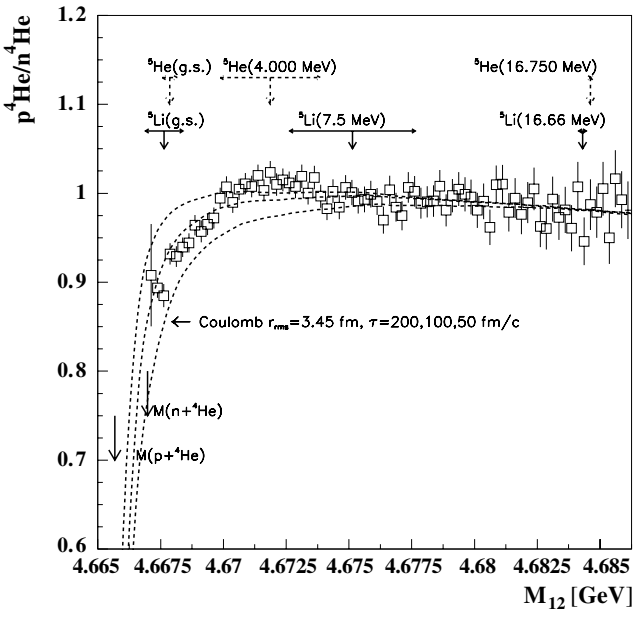

Fig. 5. The effective-mass dependence of the ratio of the p ^{4}He and n ^{4}He correlation functions.

effect of the Coulomb repulsion in the p ^{4}He system. The calculation assumed the independent emission by an exponentially decaying static source of a Gaussian spatial form [3]. The curves from right to left correspond to the root-mean-square radius $r_{\mathrm{r.m.s.}} = 3.45$ fm (the radius of ^{40}Ar) and the mean emission time $\tau = 50, 100$ and 200 fm/c. To account for a nonconstant behaviour of the ratio at $M_{12} > 4.675$ GeV, we have multiplied the theoretical curves by a linear function $C_1 + C_2 \cdot M_{12}$ and fitted the experimental ratio by this dependence. The nonzero slope value $C_2 \approx 3$ GeV^{-1} may arise due to technical and physical reasons. The estimated mean emission time $\tau \sim 100$ fm/c. Some differences between the fitted and the experimental ratio of the p ^{4}He and n ^{4}He correlation functions may be due to several reasons:

a) the assumption of factorization of strong and Coulomb interaction is not completely true;

b) the two-particle CFs can be influenced by three-body decays (*i.e.*: $^6\mathrm{He} \to {}^4\mathrm{He} + \mathrm{n} + \mathrm{n}$, $^9\mathrm{B} \to \mathrm{p} + {}^8\mathrm{Be} \to {}^4\mathrm{He} + {}^4\mathrm{He} + \mathrm{p}$);

c) the influence of the experimental cut-off for n, p and ^{4}He;

d) the neglect of stopping power corrections for p and ^{4}He.

Figure 6 shows the M_{12}-dependence of the nT and p ^{3}He correlation functions. The shapes of these correlation functions are similar: both of them show no narrow peaks and a suppression at small relative momenta. The latter effect is particularly nontrivial for the nT system because of the absence of the Coulomb repulsion. It should be noted, that both p ^{3}He and nT add up to exotic nuclei (^{4}Li and ^{4}H, respectively). The known excited states of ^{4}Li and ^{4}H [13] are shown in fig. 6. All these excited states are wide, so the absence of narrow peaks in the correlation function seems to be justified. Moreover, one can suppose that the production of the exotic nuclei in the systems p ^{3}He and nT is suppressed. Following Friedman [14], we can suppose that these cross-sections do not correspond to the chemical and thermal equilibrium. Then, we can assume that the yields of ^{4}Li(^{4}H) and its excited states are not directly linked to the actual space-time parameters of the interaction.

Within the theory of the final-state interaction, a suppression of the correlation function near the threshold corresponds to a negative value of the scattering length (defined as the scattering amplitude at $k^* = 0$). In the case of

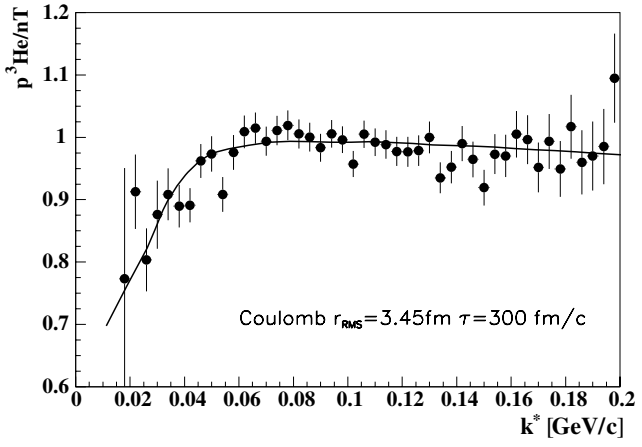

Fig. 7. The k^*-dependence of the ratio of the p ^{3}He and nT correlation functions.

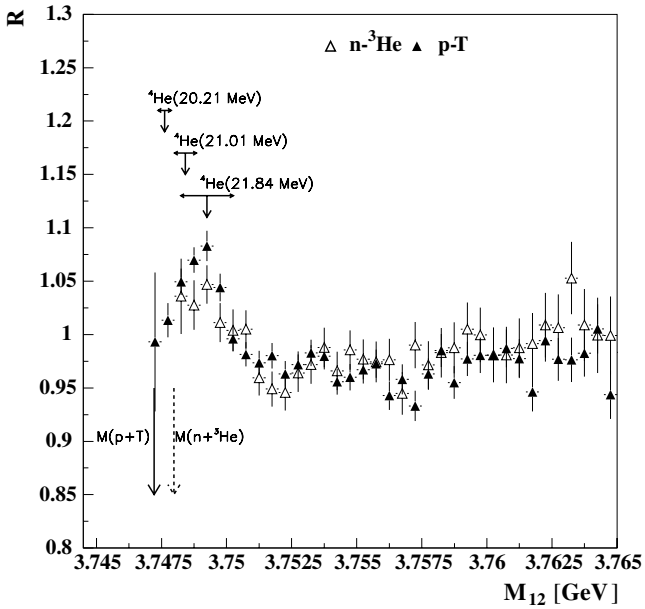

Fig. 8. The effective-mass dependence of the pT and n ^{3}He correlation functions.

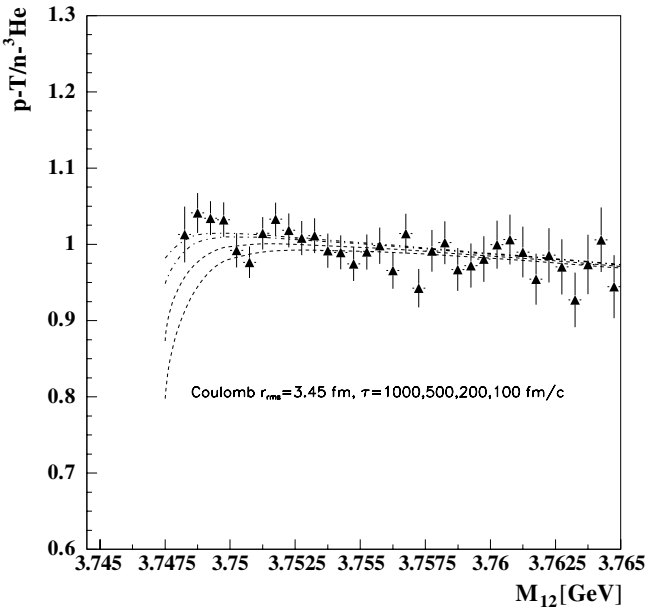

Fig. 9. The effective-mass dependence of the ratio of the pT and n ^{3}He correlation functions.

composite particles containing identical fermions one can try to explain the suppression at small relative momenta (and so the negative scattering length) based on the quantum statistics. Indeed, considering T as a system of quasi-free nucleons, the nT system will provide 3 neutrons with approximately the same momenta within the interaction volume. The correlation function for the system of 4 nucleons, nnnp, should thus decrease near the threshold due to Fermi statistics. The width of the effect in k^* should be inversely related to the space-time parameters of the production region. The experimental data can be tested for the conformity with this interpretation. Let us compare our nT correlation data with the parameterization: $P_1(1-P_2\exp(-k^{*2}P_3^2/(4\hbar c)^2))$, widely used for the description of the interferometry phenomena (see, for example, [9]). The parameter P_3 up to a factor of two corresponds to the root-mean-square radius of the interaction region. The estimation of this parameter using the nT correlation function gives P_3 about 15 fm which corresponds to the same order of magnitude for emission time as for p ^{4}He (n ^{4}He).

Figure 7 shows the ratio of the p ^{3}He and nT correlation functions *versus* pair relative momentum k^*. We assume that the main contribution to the ratio is the Coulomb interaction between p and ^{3}He. The curve on this figure corresponds to the Coulomb contribution to the p ^{3}He correlation function at $r_{\mathrm{r.m.s.}} = 3.45$ fm and $\tau = 300$ fm/c. The mean emission times of 300 fm/c reasonable and up to a factor of three coincides with τ deduced from p ^{4}He (n ^{4}He) and nT data.

The effective-mass dependence of the n ^{3}He and pT correlation functions is shown in fig. 8. These pairs are related with the nucleus ^{4}He that has a larger production cross-section compared with the unstable isotopes analyzed above. One can see the increase of the correlation functions in the region of excited states of ^{4}He: near 20.21, 21.01 and 21.84 MeV [13]. There are two reasons for the difference between the n ^{3}He and pT correlation functions. First, the Coulomb repulsion is absent for the n ^{3}He system. Second, the pT correlation due to the resonances is enhanced by larger phase space. It looks like these two effects compensate each other and thus both correlation functions become similar. If so, the assumption of the same effect of the strong final-state interaction on the n ^{3}He and pT correlation functions could lead to the overestimation of the effective source size (lifetime).

The effective-mass dependence of the ratio of the pT and n ^{3}He correlation functions is shown in fig. 9. This ratio is compared with the effect of the Coulomb repulsion in the pT system in the same way as for the p ^{4}He system (with the same slope parameter $C_2 = 3$ GeV^{-1} in the factor $C_1 + C_2 \cdot M_{12}$). The curves from up to down correspond

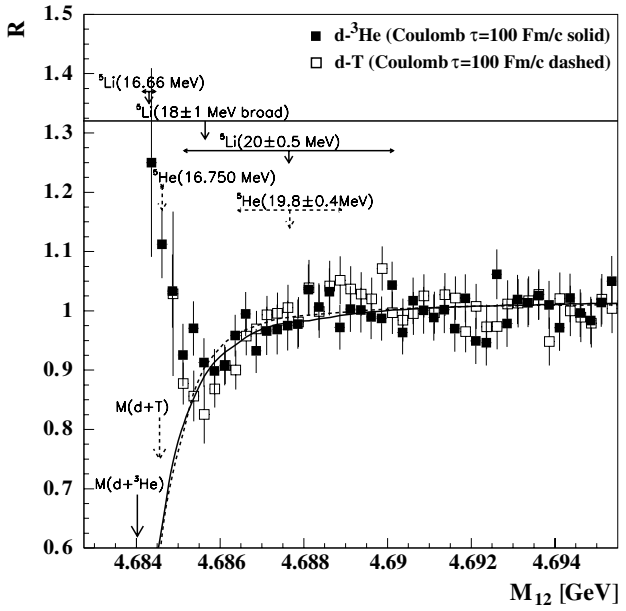

Fig. 10. The effective-mass dependence of the d ^{3}He and dT correlation functions.

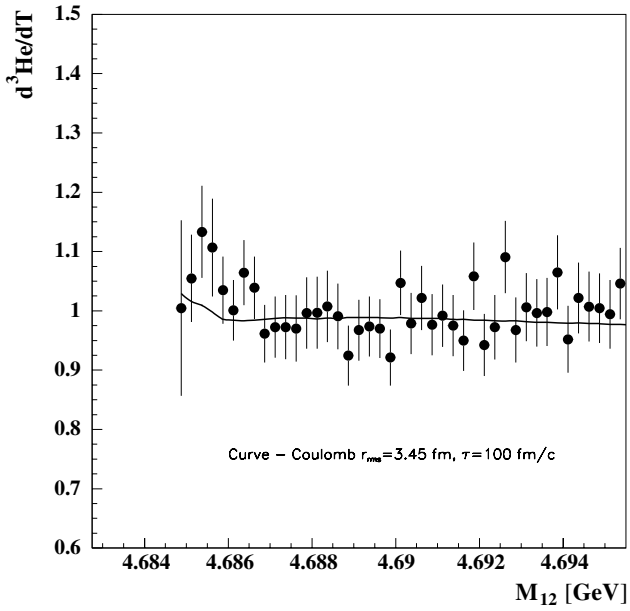

Fig. 11. The effective-mass dependence of the ratio of the d ^{3}He and dT correlation functions.

to the source root-mean-square radius $r_{\mathrm{r.m.s.}} = 3.45$ fm and the mean emission times $\tau = 1000, 500, 200$ and 100 fm/c. The flat behaviour of the experimental ratio points to the emission time larger than 200 fm/c, *i.e.* at least by a factor of two larger than for p ^{4}He (n ^{4}He). One should however take into account a possible overestimation of the time parameter due to the compensation effect discussed above.

Figure 10 shows the effective-mass dependence of the d ^{3}He and dT correlation functions. Both correlation functions have a minimum at $M_{12} \sim 4.686$ GeV and show no significant structures for $M_{12} > 4.688$ GeV. The data are compared with the Coulomb d ^{3}He (solid curve) and dT (dashed curve) correlation functions calculated with the source size parameter $r_{\mathrm{r.m.s.}} = 3.45$ fm and the emission time $\tau = 100$ fm/c. An agreement is seen except for the peak present in the data at small M_{12} that is probably related with the excited states of ^{5}Li (d ^{3}He) at 16.66 MeV and of ^{5}He (dT) at 16.70 MeV [13]. Similar peaks were observed for d ^{3}He [10] and dT [11] systems. Figure 11 presents the ratio of the d ^{3}He and dT correlation functions. The curve shows the ratio of the Coulomb correlation functions for these pairs with the emission time $\tau = 100$ fm/c and $r_{\mathrm{r.m.s.}} = 3.45$ fm. The experimental data do not contradict with the ratio of the above Coulomb correlation functions thus indicating the mean emission time of about 100 fm/c for the particles in these pairs.

Collecting the results for different pairs, we may estimate the mean emission time τ of the low-mass fragments in the reaction ^{40}Ar + ^{58}Ni at 77 MeV/nucleon as 100–350 fm/c. It should be noted that theoretical correlation functions were computed for the source radius $r_{\mathrm{r.m.s.}} = 3.45$ fm (the radius of ^{40}Ar). This value should evidently be considered as an upper limit of real source dimension. But for our study it is not crucial because the time contribution to the measured space-time interval is the dominant one. The estimation of the emission time proved to be the same within errors for a source radius of 2 fm.

The mean emission time of the low-mass fragments in the reaction ^{40}Ar + ^{58}Ni at 77 MeV/nucleon is much less than the mean neutron emission time deduced from the two-neutron correlation function [15] in the same experiment.

The estimates of the mean emission time from the central intermediate-energy heavy-ion collisions [16] are close to our results.

4 Conclusions

1) A new approach has been proposed to study the correlations of the fragments and particles at small relative momenta. This approach is based on the comparison of the correlation functions of the isosymmetrical pairs. The main reason for using these systems is an attempt to separate up, to some extent, the different contributions to the correlation functions.

2) For the first time, we have the experimental evidence that the Fermi statistics applied to nucleons in bound systems suppresses the correlations of these systems at small relative momenta.

3) There are experimental evidences that the balance between the production cross-sections for nuclei and their fragments is disrupted at least in some cases: the production cross-section seems to be lower than the equilibrium values for the exotic nuclei (^{4}Li and ^{4}H), while for ^{4}He it seems to be higher than in the equilibrium.

4) The values of the emission time parameter have been extracted for different particle species. They appear to be consistent and in agreement with previous data.

References

1. G.I. Kopylov, M.I. Podgoretsky, Sov. J. Nucl. Phys. **15**, 219 (1972); M.I. Podgoretsky, Sov. J. Nucl. Phys. **20**, 266 (1989).
2. S.E. Koonin, Phys. Lett. B **70**, 43 (1977); S. Pratt, M.B. Tsang, Phys. Rev. C **36**, 2390 (1987).
3. R. Lednicky, V.L. Lyuboshitz, Sov. J. Nucl. Phys. **35**, 770 (1982).
4. D.H. Boal, C.K. Gelbke, B.K. Jennings, Rev. Mod. Phys. **62**, 553 (1990).
5. I. Tilquin *et al.*, Nucl. Instrum. Methods A **365**, 446 (1995).
6. J. Pluta *et al.*, Nucl. Instrum. Methods A **411**, 417 (1998).
7. M. Przewlocki *et al.*, Acta Phys. Pol. B **31**, 379 (2000).
8. I. Juricic *et al.*, Phys. Rev. D **39**, 1 (1989); Yu.D. Bayukov *et al.*, Sov. J. Nucl. Phys. **52**, 305 (1990); H. Appelshauser *et al.*, Eur. Phys. J. C **2**, 661 (1998).
9. G.I. Kopylov, Preprint JINR, **P2-7211** (1973) Dubna; Phys. Lett. B **50**, 472 (1974).
10. V. Serfling *et al.*, Phys. Rev. Lett. **80**, 3928 (1998).
11. Zhi Yong He *et al.*, Nucl. Phys. A **620**, 214 (1997).
12. R. Kotte *et al.*, Eur. Phys. J. A **6**, 185 (1999).
13. S. Fiarman, W.E. Meyerhof, Nucl. Phys. A **206**, 1 (1973); F. Ajzenberg-Selove, Nucl. Phys. A **490**, 1 (1988); D.R. Tilley, H.R. Weller, G.M. Hale, Nucl. Phys. A **541**, 1 (1992).
14. William A. Friedman, Phys. Rev. C **60**, 014601 (1999).
15. K. Wosinska *et al.*, Acta Phys. Pol. B **33**, 507 (2002).
16. D. Fox *et al.*, Phys. Rev. C **47**, R241 (1993).